SPHERIC 2023

Rhodes, Greece, 27-29 June

Proceedings of the 17th International SPHERIC Workshop

Editor
Georgios Fourtakas

SPHERIC 2023

Proceedings of the 17th International SPHERIC Workshop

Rhodes Island, Greece, 27-29 June 2023

Organized by:
School of Engineering
Faculty of Science and Engineering
The University of Manchester
UK

Editor
Georgios Fourtakas

Published by The University of Manchester, UK
ISBN 978-1-3999-5885-1

Acknowledgements

The 17th International SPHERIC Workshop was supported by the School of Engineering, Faculty of Science and Engineering, The University of Manchester.

The local organising committee would like to acknowledge the help and support from our colleagues in the University of Manchester. We convey our deepest and sincere gratitude to the SPHERIC Scientific and Steering Committee for their guidance, advice and assistance, without them none of this would have ever been possible.

We would like to say a special thank you to Dr Aaron English for creating our SPHERIC 2023 logo and helping us with the organisation of the workshop.

Foreword

Dear Delegate,

Since its conception in 2005 with the Inaugural Meeting in Chatou, France, the Smoothed Particle Hydrodynamics rEsearch and Engineering International Community (SPHERIC) has foster, steered and disseminated the development and application of the Smoothed Particle Hydrodynamics (SPH) method in academia and industry alike.

The International SPHERIC Workshops are a unique series of yearly events with exclusive focus on the SPH method and associated particle-based methods. SPH has been widely adopted in the field of computational fluid mechanics, solid mechanics, geomechanics, manufacturing engineering and many other disciplines. The SPH scheme is considered to be the mainstream method for free-surface flows, and multi-phase flows, high non-linear deformation, fracture and fragmentation and, complex physics due to its meshless particle-based nature.

The SPHERIC workshop brings together state-of-the-art developments from academia and novel interdisciplinary applications from industry in a unique blend towards the advancement of the numerical scheme.

It is our pleasure and privilege to host the 17th edition of the International SPHERIC Workshop in Rhodes Island, Greece and I am looking forward to welcoming you for a stimulating and fruitful event.

Sincerely,

Georgios Fourtakas
Chair of the Local Organizing Committee
17th International SPHERIC Workshop

Committees

Scientific Committee

Prof. Renato Vacondio (Università di Parma, Italy)
Prof. Antonio Gil (Swansea University, UK)
Prof. Raj Das (RMIT University, Australia)
Prof. Ben Rogers (University of Manchester, UK)
Dr. Georgios Fourtakas (University of Manchester, UK)
Dr. Chun Hean Lee (Universiy of Glasgow, UK)
Prof Alex Crespo (Universidade de Vigo, Ourense, Spain)
Prof. Abbas Khayyer (Kyoto University, Japan)
Prof. David Le Touzé (Ecole Centrale de Nantes, France)
Dr Nathan Quinlan (National University of Ireland, Galway, Ireland)
Dr. Xiangyu Hu (Technical University of Munich, Germany)
Dr. Pengnan Sun (Sun Yat-sen University, China)
Dr. Tom De Vuyst (University of Hertfordshire, UK)
Dr Christopher Curtis Long (Los Alamos National Laboratory, USA)
Prof. Moncho Gómez-Gesteira (Universidade de Vigo, Spain)
Prof. Xu Fei (Northwestern Polytechnical University, China)
Dr. Rouhollah Fatehi (Persian Gulf University, Iran)
Dr. Nathaniel Albert Trask (Sandia National Laboratories, USA)
Prof. Mehmet Yildiz (Sabanci University, Turkey)
Prof. Andrea Colagrossi (CNR-INM, Italy)
Dr. Matthieu De Leffe (Siemens Digital Industries, France)
Dr. Salvatore Marrone (CNR-INM, Italy)
Prof. Peter Eberhard (University of Stuttgart, Germany)
Dr. Steven Lind (University of Manchester, UK)
Mr. Pierre Sabrowski (Dive Solutions, Germany)
Dr. Giuseppe Bilotta (Istituto Nazionale di Geofisica e Vulcanologia, Italy)
Dr. Ha Bui (Monash University, Australia)
Prof. Stefano Sibilla (Università di Pavia, Italy)
Prof. Antonio Souto Iglesias (UPM, Spain)
Dr Angelo Tafuni (New Jersey Institute of Technology, US)

Local Organising Committee

Dr Georgios Fourtakas
Dr Steven Lind
Dr Abouzied Nasar
Mr Chunze Cen
Mr Ruofeng Feng
Miss Meixuan Lin
Mr Sumanta Laha

Table of contents

Multiple continua and multi-phase flows

Free surface and moving boundaries

Solids and structures

Complex flows I

Artificial intelligence and machine learning

Adaptivity & variable resolution

Boundary conditions

Hydraulic applications

Geotechnical & disaster applications

Process & manufacturing engineering applications

Complex flows II

SPH simulation of three-dimensional resonant viscous sloshing flows

C. Pilloton, J. Michel, A. Colagrossi, S. Marrone
INM Institute of marine engineering
CNR National Research Council
Rome, Italy
salvatore.marrone@cnr.it

P. Colagrossi
Punkt.ink,
Rome, Italy

***Abstract*—Three-dimensional resonant sloshing flows in a square-base tank is analysed to investigate swirling instability. To this aim a tank is harmonically forced along the horizontal x-component with frequency equal to the first resonant mode. Specifically, the influence of the viscosity on the inception of this flow instability is studied. Four different liquids characterized by different viscosity are considered: water, sunflower oil, castor oil and glycerin. In order to model these flows, an enhanced version of the SPH model called δ-LES-SPH [2] is chosen as some of the considered flows are turbulent. The adopted numerical scheme correctly reproduces the swirling regimes as theoretically predicted and experimentally observed by [16]. The particle nature of SPH allows for a straightforward and explicit analysis of energy terms during the flow evolution. The sloshing related energy damping, therefore, can be directly measured. Further, the considered phenomenon requires the simulation of several tens of periods. In this respect, the adoption of SPH is an advantage thanks to the exact mass conservation and the accurate modelling of the complex free-surface deformations. The present investigation underlines the strict relation between the energy dissipation and the swirling instability, showing that more energy is dissipated when swirling motion is activated and wave breaking events occur. It is also shown that liquids characterized by lower viscosity are more prone to develop a swirling instability.**

I. Introduction

Sloshing flow phenomena may appear in partially filled tanks produced by the motion of vehicles as ships, aircraft, spacecrafts, rockets and satellites, or in containers as a consequence of earthquakes. In turn, the raising of internal waves may cause impact loads, influencing the vehicle's motion and the structure dynamics in their mutual interaction. In recent decades, sloshing flows have been widely investigated with analytical, experimental and numerical methods.

Sloshing phenomena are deeply analysed in the book by [15], where a particular attention is referred to the land-based and marine applications focusing on ship tanks. Although three-dimensional flow studies are not widespread in the literature, it is well known that the fluid can evolve in plane waves, rotational motion or in a chaotic solution, depending on the tank aspect ratio, the filling height, the oscillation frequency and the direction of the forced motion. In particular, when sloshing waves move in a clockwise or counterclockwise direction along the tank walls, this kind of motion is called "swirling" and it is a special feature of 3D sloshing flow that may take place in vertical cylinder, spherical, square-base or nearly square-base tanks when they oscillate with a forcing frequencies near to the resonant one.

Sloshing in a circular cylinder with a slowly rotating liquid has been experimentally and theoretically investigated in [35] for aquaculture fish farm. In particular it is shown that liquid rotation is able to modify the sloshing resonant regimes and for some specific conditions the unwanted swirling instability can be suppressed. An intense examination of resonant three-dimensional nonlinear sloshing in a square-base basin with finite depth is reported, *e.g.*, in [14], [13]. Starting from the potential flow method, the approach of primitive variables is described in the case of fully nonlinear effects of the waves on the free surface and supported by experimental results. In [17] the effect of viscosity was investigated experimentally in sloshing flow in intermediate liquid depth. The free-surface profiles of low and high viscous fluids under resonant excitation are analysed in connection with the dynamic pressures and excitation accelerations. A further numerical investigation on a squared tank forced with a coupled surge-sway motion under various oblique excitation angles and water depths was recently made by [37], studying in depth the evolution of swirling waves during the initial transient stage in terms of kinematic, dynamic and energy characteristics of sloshing waves. The mechanism of swirling phenomenon is still not clear but its evolution seems to be very sensitive to the physical conditions as tank geometry, the filling height, the excitation frequency, the amplitude and the angle of external forcing.

The present work is dedicated to the numerical analysis through SPH of the swirling instability and, in particular, of the influence by the fluid viscosity, employing four different fluids inside a square-base 3D tank with a filling ratio of about 50%. The tank is forced horizontally along one of the tank edge at the first resonant frequency. The liquids considered are water, sunflower oil, castor oil and glycerine, the associated Reynolds numbers range from 214.8 up to 253,100, covering four orders of magnitude. As expected it is shown that when increasing the viscosity the swirling instability is delayed in time, and specifically we found that when using the glycerine the swirling mode is completely suppressed. The energy dissipated associated with the sloshing flow is also studied. It is shown that when the

swirling instability is excited the slosh dissipation increases. Besides this, it is found that the highest slosh dissipation is obtained with liquids characterised by lower viscosity, as already demonstrated in other sloshing studies (see *e.g.* [7], [8], [27]). This is linked with the fragmentation phenomena occurring at higher Reynolds numbers which induce a larger energy dissipation. The numerical simulation performed with water refers to an experiment described in [16], where the swirling instability is excited choosing a horizontal periodical motion with a frequency that is close to the lowest natural frequency. Thanks to the conservation properties of the SPH, this numerical method is particular suitable for simulating long-time evolution [31]. In particular in this work an enhanced model called δ-LES-SPH is adopted. The latter has been demonstrated to be suitable for the simulation of violent sloshing flow and associated damping, see *e.g.* [27], [24].

The paper is arranged as follows:

- Sec. II introduces the governing equations and the δ-LES-SPH model are briefly recalled. The evaluation of the slosh dissipation is also discussed.
- Sec. III is devoted to introduce the test-case simulated varying the fluid inside the 3D square-base tank. Numerical results are presented, underling the effects of fluid viscosity and the dissipation process. Comparison of the free-surface configurations, time histories of the mechanical energy and orbital evolution of the horizontal force components are presented.

II. Adopted model and numerical approximation

A. Governing equations

The governing equation used for modelling the sloshing flow in the present work are the Navier-Stokes equations. Only the liquid phase is modelled, thermal conductivity and surface tension can be neglected for the specific problem at hand. Furthermore, the liquid is assumed to be a weakly compressible medium. The tank is assumed to translate along the x-axis. The equation are formulated in the non-inertial frame of reference (Ni-FoR). With these assumptions, the flow evolution is governed by:

$$\begin{cases} \dfrac{D\rho}{Dt} = -\rho\,\mathrm{div}(\boldsymbol{u}), \qquad \rho\dfrac{D\boldsymbol{u}}{Dt} = \mathrm{div}(\mathbb{T}) + \rho\boldsymbol{g} - \rho a_{tank}(t)\,\boldsymbol{i} \\ \dfrac{De}{Dt} = \dfrac{\mathbb{T}:\mathbb{D}}{\rho}, \qquad \dfrac{D\boldsymbol{r}}{Dt} = \boldsymbol{u}, \qquad p = f(\rho) \end{cases}$$

where D/Dt represents the Lagrangian derivative, $\boldsymbol{u}$ the fluid velocity, ρ the liquid density, $\boldsymbol{g}$ the gravitational acceleration, $a_{tank}(t)$ the tank acceleration, $\boldsymbol{i}$ the unit vector of the x-axis, $\mathbb{T}$ the stress tensor, e the specific internal energy, $\mathbb{D}$ the rate of stress tensor and $\boldsymbol{r}$ the position of material point.

The liquid is assumed to be Newtonian and the flow isothermal *i.e*: $\mathbb{T} = [-p + \lambda\,\mathrm{div}(\boldsymbol{u})]\,\mathbb{I} + 2\,\mu\,\mathbb{D}$, where μ and λ are the primary and secondary dynamic viscosity of the liquid and $\mathbb{I}$ is the identity tensor. The liquid is assumed also as barotropic and therefore the pressure depends on the density exclusively. As a consequence the internal energy equation in (1) is decoupled by the momentum equation and it is used just to control the energy conservation of the numerical scheme.

The assumption of small density variations allows for using a linear equation of state

$$p = c_0^2\,(\rho - \rho_0)$$

where ρ_0 is the density at the free surface and c_0 is the speed of sound. By considering that the time integration is performed with a time step related to the value of c_0, the latter is always set lower than its physical counterpart (in the present work, about two orders of magnitude lower). The weakly-compressible regime is always guaranteed by the condition:

$$c_0 \geq 10\,\max\Big(U_{max}\,,\,\sqrt{(\Delta p)_{max}/\rho}\Big), \tag{2}$$

where U_{max} and $(\Delta p)_{max}$ stand respectively for the expected maximum velocity and pressure variation within the fluid domain.

B. The δ-LES-SPH scheme

Following in [23], [27], [21] in the present work the δ-LES-SPH scheme derived in [2], [25] is used to approximate equation (1). The main characteristics of the scheme are recalled here and for specifics the interested reader is referred to the above-mentioned articles. In order to recover regular spatial distribution of particles and consequently accurate approximation of the SPH operators [32], [29], a Particle Shifting Technique (PST) is used (see also *e.g.* [18]). For the sake of brevity the specific law adopted for the shifting velocity $\delta\boldsymbol{u}$ is not reported here, this being identical to the one adopted by [23], [27] in which violent sloshing problems were studied.

This PST velocity is then taken into account within the continuity and momentum equations rewriting the governing equations (1) in a quasi-Lagrangian formalism:

$$\frac{d(\bullet)}{dt} := \frac{\partial(\bullet)}{\partial t} + \nabla(\bullet)\cdot(\boldsymbol{u} + \delta\boldsymbol{u})$$

and the resulting SPH schemes reads as:

$$(1)\begin{cases} \dfrac{\mathrm{d}\rho_i}{\mathrm{d}t} = -\rho_i\,\mathrm{div}(\boldsymbol{u}_i + \delta\boldsymbol{u}_i) + \mathrm{div}(\rho_i\delta\boldsymbol{u}_i) + \mathcal{D}_i^{\rho} \\ \dfrac{\mathrm{d}\boldsymbol{u}_i}{\mathrm{d}t} = -\dfrac{\boldsymbol{\nabla}p_i}{\rho_i} + \dfrac{\mathrm{div}\,(\rho_i\boldsymbol{u}_i\otimes\delta\boldsymbol{u}_i)}{\rho_i} + \boldsymbol{F}_i^{v} + \boldsymbol{g} + a_{tank}(t)\,\boldsymbol{i} \\ \dfrac{\mathrm{d}\boldsymbol{r}_i}{\mathrm{d}t} = \boldsymbol{u}_i + \delta\boldsymbol{u}_i, \quad V_i(t) = m_i\,/\rho_i(t), \quad p_i = c_0^2(\rho_i - \rho_0) \end{cases} \tag{3}$$

where m_i and $\boldsymbol{F}_i^v$ are the mass and the net viscous force related to the i-th particle, while $\mathcal{D}_i^{\rho}$ is a numerical diffusive term for stabilising the numerical scheme avoiding spurious noise in the pressure field. For the sake of brevity $\mathcal{D}_i^{\rho}$ is not reported here, the interested reader can find more details in [1] and more specifically in [2], [25] where the intensity of this term is determined dynamically in space and time.

The spatial differential operators are approximated by:

$$\begin{cases} \mathrm{div}(\boldsymbol{u}_i + \delta\boldsymbol{u}_i) &= \sum_j [(\boldsymbol{u}_j + \delta\boldsymbol{u}_j) - (\boldsymbol{u}_i + \delta\boldsymbol{u}_i)] \cdot \boldsymbol{\nabla}_i W_{ij} V_j \\ \mathrm{div}(\rho_i \delta\boldsymbol{u}_i) &= \sum_j (\rho_i \delta\boldsymbol{u}_i + \rho_j \delta\boldsymbol{u}_j) \cdot \boldsymbol{\nabla}_i W_{ij} V_j \\ \boldsymbol{\nabla} p_i &= \sum_j (p_i + p_j) \boldsymbol{\nabla}_i W_{ij} V_j \\ \mathrm{div}(\rho_i \boldsymbol{u}_i \otimes \delta\boldsymbol{u}_i) &= \sum_j (\rho_i \boldsymbol{u}_i \otimes \delta\boldsymbol{u}_i + \rho_j \boldsymbol{u}_j \otimes \delta\boldsymbol{u}_j) \boldsymbol{\nabla}_i W_{ij} V_j \,, \end{cases}$$

where the j index refers to neighbour particles of i-th particle. The spatial gradients are approximated through the convolution with a kernel function W_{ij}. A C2-Wendland kernel is adopted in the present work (see [36]).

Initially the particles are distributed on a Cartesian lattice with spacing Δx, consequently the volumes V_{i0} at time $t = 0$, are initialised as Δx^3. Regarding the radius of the support of the kernel W, this is fixed to $2h = 2.7\Delta x$, being h the smoothing length.

The particle masses m_i are calculated through the initial pressure field, *i.e* $m_i = \rho_{i0}, V_{i0}$ and they remain constant during the time evolution; while the volumes V_i change in time accordingly with the particle density, *i.e.* $V_i(t) = m_i/\rho_i(t)$.

The viscous force acting on particle i is computed through Monaghan formulation [28] and contains both the effect of the physical viscosity μ and the turbulent stresses μ_i^T (see also [19], [33]):

$$\begin{cases} \boldsymbol{F}_i^v &:= \dfrac{10}{\rho_i} \displaystyle\sum_j (\mu + \mu_{ij}^T) \pi_{ij} \nabla_i W_{ij} V_j \\ \pi_{ij} &:= \dfrac{(\boldsymbol{u}_i - \boldsymbol{u}_j) \cdot (\boldsymbol{r}_i - \boldsymbol{r}_j)}{\|\boldsymbol{r}_i - \boldsymbol{r}_j\|^2}, \qquad \mu_{ij}^T := 2\, \dfrac{\mu_i^T \mu_j^T}{\mu_i^T + \mu_j^T} \end{cases} \tag{4}$$

where C_S is the Smagorinsky constant, set equal to 0.18 (see [34], [6]), while $\mu_i^T := \rho_0 (C_S\, 2h)^2 \|\mathbb{D}_i\|$ being $\|\mathbb{D}\| = \sqrt{2\mathbb{D} : \mathbb{D}}$ and velocity gradients evaluated through an MLS interpolation. In the present work the subgrid model for the turbulent viscosity is needed because of the high Reynolds number related to the simulations with water. More details related to the LES modelling rewritten in a quasi-Lagrangian formalism can be found in [2].

Finally, the scheme is integrated in time using a 4th-order Runge-Kutta scheme for which the time-step Δt is obtained by means of CFL conditions:

$$\Delta t = \min\left(0.031 \min_i \frac{(2h)^2 \rho_i}{(\mu + \mu_i^T)}, \quad 0.3 \min_i \sqrt{\frac{\Delta r}{\|\boldsymbol{a}_i\|}}, \quad 0.6\, \frac{2h}{c_0} \right)$$

where $\|\boldsymbol{a}_i\|$ is the particle acceleration. Even for the lowest Reynolds number considered in the present article, the last two constraints are always dominant with respect to the first one related to the viscous diffusion process.

C. Enforcement of the boundary conditions

The solution of the governing equations (1) requires the definition of the boundary conditions on the free surface and on the tank walls. As discussed in [10], [11], the kinematic and dynamic conditions of the free surface are intrinsically satisfied in SPH methods.

The adherence boundary condition on the solid surface can be enforced through a ghost-fluid approach (see *e.g.* [20] [3] and also [4], [30] when quasi-Lagrangian formulation is used). The latter requires that at least five particles should be present within the boundary layer region. An estimation of the wall boundary thickness (WBT) can be obtained using the Blasius equation, and for the water test-case (Reynolds number is about 250,000) it results that the WBT is less than one millimetre and at the maximum spatial resolution only one SPH particle is present in the boundary layer region. For this reason the free-slip condition is enforced for the water test-case while for the other three liquids the no-slip condition can be applied. Similar hypothesis was also used in previous works [22], [27], [21].

D. Evaluation of the slosh dissipation

Following the analysis performed in [23], [27], the δ-LES-SPH energy balance can be written as:

$$\begin{cases} \dot{\mathcal{E}}_K + \dot{\mathcal{E}}_P - \mathcal{P}_{NF} = \mathcal{P}_V + \mathcal{P}_V^{turb} + \mathcal{P}_N \\ \mathcal{E}_K(t) = \dfrac{1}{2} \displaystyle\sum_i m_i\, u_i^2\,, \quad \mathcal{E}_P(t) = \sum_i m_i\, g\, z_i \\ \mathcal{P}_{NF} = \displaystyle\sum_i m_i\, a_{tank}(t)\, \boldsymbol{i} \cdot \boldsymbol{u}_i \end{cases} \tag{5}$$

where on the left-hand side, $\mathcal{E}_K$ and $\mathcal{E}_P$ are the kinetic and potential energy of the particle system. For $\mathcal{E}_P$ the vertical position of the generic i-th particle is indicated with z_i. $\mathcal{P}_{NF}$ is the power linked to the non-inertial forces.

The elastic potential energy linked to the compressibility of the liquid is negligible within the weakly-compressible assumption; hence, it is not considered in the energy balance (for more details see [5]).

The right-hand side of the energy balance (5) contains the dissipation terms due to the real viscosity $\mathcal{P}_V$, to the turbulent viscosity $\mathcal{P}_V^{turb}$, while $\mathcal{P}_N$ takes into account the effect of the density diffusion and the particle shifting $\delta\boldsymbol{u}$ (see [26]). The power related to the viscous forces is directly evaluated through the expression (4) as:

$$\mathcal{P}_V + \mathcal{P}_V^{turb} = 5 \sum_i \sum_j (\,\mu + \mu_{ij}^T\,)\, \pi_{ij}\, (\boldsymbol{u}_i - \boldsymbol{u}_j) \cdot \nabla_i W_{ij}\, V_i\, V_j \tag{6}$$

where the quantity $\mathcal{P}_V^{turb}$ refers to the viscous dissipation of the modelled sub-grid scales, whereas $\mathcal{P}_V$ refers to the resolved scales.

The energy dissipated by the fluid is then evaluated by integrating time into equation (5):

$$\begin{cases} [\mathcal{E}_K + \mathcal{E}_P](t) - [\mathcal{E}_K + \mathcal{E}_P](t_0) - \mathcal{W}_{NF}(t) = \mathcal{E}_{diss}(t) \\ \mathcal{W}_{NF}(t) = \displaystyle\int_{t_0}^{t} \left[\sum_i m_i\, (-a_{tank}\, \boldsymbol{i} \cdot \boldsymbol{u}_i) \right] dt \\ \mathcal{E}_{diss}(t) = \displaystyle\int_{t_0}^{t} \left(\mathcal{P}_V + \mathcal{P}_V^{turb} + \mathcal{P}_N \right) dt \end{cases} \tag{7}$$

where W_{NF} is the work performed by the non-inertial forces on the fluid and $[\mathcal{E}_K + \mathcal{E}_P](t_0)$ is the mechanical energy related to the time instant t_0.

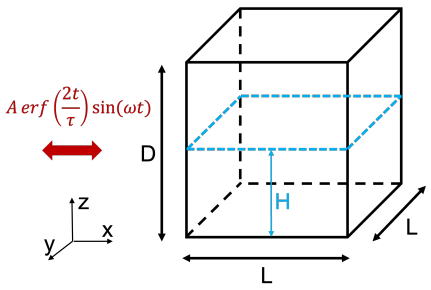

L [cm]	59
W [cm]	59
D [cm]	89
H [cm]	30
A [cm]	0.92
T [s]	0.9059

Fig. 1. Left:Sketch of the tank. Right: geometric tank sizes of the experiments by [14], amplitude A and period T of the harmonic tank motion imposed.

Test	Label	m_l (Kg)	ν (m/s^2)	$\Delta\mathcal{E}$ (J)	Re = $\frac{\sqrt{gH}\,H}{\nu}$
1	Water	104.1	$1.02\,10^{-6}$	153.1	253,100
2	Sunflower Oil	131.7	$4.99\,10^{-5}$	138.9	5155
3	Castor Oil	93.9	$1.04\,10^{-4}$	147.4	2469
4	Glycerin	100.3	$1.20\,10^{-3}$	193.6	214.8

TABLE I

TEST CASE MATRIX: m_l IS THE TOTAL LIQUID MASS, ν THE KINEMATIC VISCOSITY, $\Delta\mathcal{E}$ THE REFERENCE ENERGY (INITIAL POTENTIAL ENERGY WITH RESPECT THE TANK BOTTOM $\Delta\mathcal{E} = 1/2\, m_l\, g\, H$) AND RE THE REYNOLDS NUMBER OF THE SLOSHING FLOW.

The first equation of (7) provides two ways for the evaluation of the energy dissipated by the fluid: (i) the first is using the left-hand side of the first equation; (ii) a second way is to directly estimate $\mathcal{E}_{diss}$ using the second equation in which the three dissipation terms are integrated in time. Both these approaches were adopted in the present simulations in order to verify that the present model is able to close the energy balance accurately (see also *e.g.*, [21], [24]).

III. Numerical results

A. Description of the test-case

In the present work, the experimental test-case analysed in [16] is considered. A square-base tank is adopted with length, width and height denoted with L, W and D which values are reported in Fig. 1. The filling height is set equal to $H = 0.508\,L$. The tank is forced to oscillate in the horizontal x direction with a prescribed time law:

$$x_{tank}(t) = A(t)\,\sin\left(\frac{2\,\pi\,t}{T}\right), \qquad A(t) = A\,\mathrm{erf}\left(\frac{2t}{\tau}\right) \tag{8}$$

where the maximum amplitude A is equal to $0.0156L$ and the ramp time $\tau = 15\,T$, which means that $A(t)$ practically reaches its maximum value A after 15 oscillation periods. The oscillation period T is set equal to the lowest natural one $T_1 = 0.9059$ seconds. The final time of the simulation is equal to $t_{fin} = 85\,T$. Four different liquids are considered: water, sunflower oil, castor oil and glycerin. Table I reports the liquid mass m_l, the kinematic viscosity ν (at temperature 25°C), the reference energy and power $\Delta\mathcal{E}$ and the Reynolds number (defined as Re = $\sqrt{gH}\,H/\nu$) related to the different liquids.

B. Flow regimes and features

In this section the different sloshing regimes developed during the 85 oscillation periods are discussed for the four different liquids. In order to identify those regimes, the time histories of the mechanical energy $\mathcal{E}_M$ of the fluids (*i.e.* sum of kinetic and potential energy) is analysed. Fig. 2 reports the time histories of $\mathcal{E}_M$ for the four liquids. The top plot refers to the water test-case. It is possible to see that $\mathcal{E}_M$ exhibits a complex behaviour in time. We identify the first regime I, where the mechanical energy increases up to a maximum

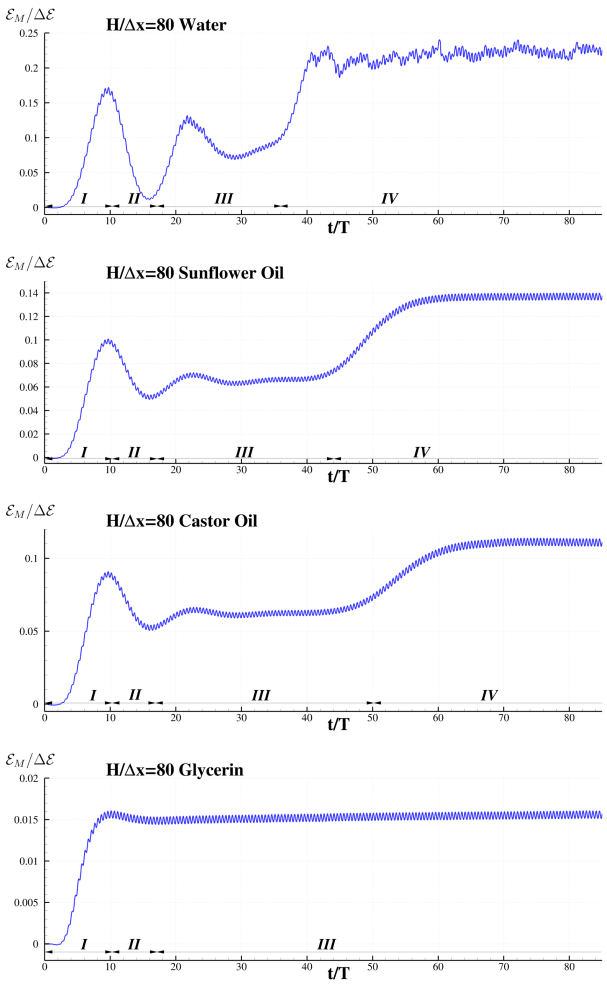

Fig. 2. Time histories of the mechanical energy for the four different liquids at the maximum spatial resolution $H/\Delta x = 80$.

value. This time is close to the end of the time ramp of the tank motion (see eq. (8)).

Within this first regime the tank walls act a positive work which is directly converted in an increase of the liquid motion inside the tank (see Sec. II-D), *i.e.*, $\mathcal{W}_{NF}(t_I) > 0$ where t_I is the end time of the regime I. Increasing the liquid viscosity,

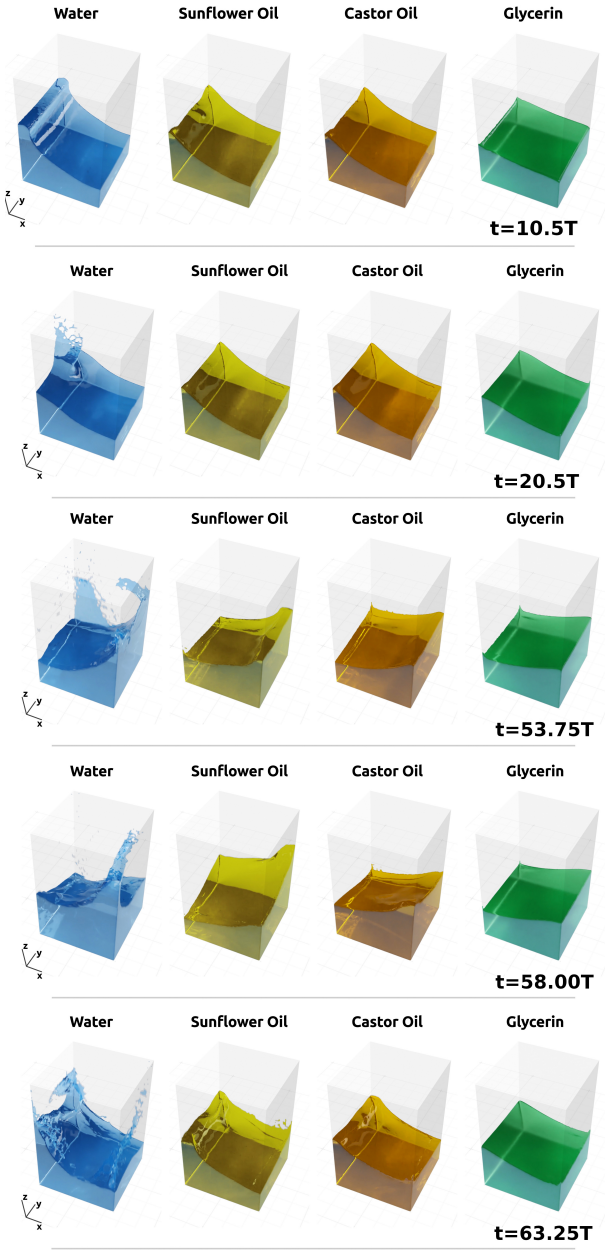

Fig. 3. Free-surface configurations for time instants $10.50T$, $20.50T$, $53.75T$, $58.00T$ and $63.25T$ for the four different liquids. The full video of the simulation is available at https://youtu.be/pCjyEY3BkTI.

the maximum of $\mathcal{E}_M$ reached in the regime I decreases because of the reduction of the liquid motion. The first row of Fig. 3 shows the free surface configuration at the end of the regime I for the four different liquids.

The second regime II is quite counter-intuitive since the mechanical energy largely decreases. For the water test-case it reaches a minimum value close to zero which means that the liquid motion inside the tank almost stops. In this regime the liquid returns the energy accumulated during the stage I to the tank walls, that is, the tank walls act a negative work on the fluid *i.e.*, $\mathcal{W}_{NF}(t_I I) - \mathcal{W}_{NF}(t_I) < 0$.

During the regime III the mechanical energy of the fluid increases again for all the fluids except for the glycerin where $\mathcal{E}_M$ oscillates around a constant value. For the water test-case the sloshing motion becomes more violent than the regime I, as displayed in the second row of Fig. 3. A transverse symmetric wave system (y direction) is generated whose wave length is half of the tank size. The amplitude of this transverse wave system increases in time and, eventually, the jet run-up on the tank edges collapses giving rise to the first breaking event in correspondence of the edge middle point. This behaviour is also documented experimentally in [14].

Finally, the regime IV is the last one recorded where the swirling wave instability takes place. This regime does not appear only in the glycerin test-case where the high viscous level inhibits this instability (see Fig. 3). In the water test-case the swirling mode is characterised by a violent motion of the free surface with the occurrence of roof impacts and several breaking events. The latter are also observed for the sunflower oil test-case but in smaller number and considerably less energetic. Conversely, for the castor oil test case the swirling occurs without any breaking events. In the water and the castor oil test-case clockwise swirling waves take place, while for the sunflower oil anticlockwise motion occurs. As also commented in [9] the direction of rotation depends on the ramp $A(t)$ (see eq. (8)) and, numerically, can also depend on parameters such as the spatial resolution $N = H/\Delta x$.

C. Forces and tank motion

A further comparison is performed on the horizontal force components to describe the different behaviour of the four fluids. The different regimes previously described in Sec. III-B are also distinguishable in Fig. 4, in particular for the water test-case.

Differently from the F_x component, which is related to the tank motion and the work exchanged between liquid and the walls, the F_y component is strictly connected with the onset of the swirling instability caused by the transition from planar wave (2D wave oscillating in x direction) to rotational ones. Looking at F_y evolution, the instability firstly starts in the water test-case, followed by sunflower and castor oil. In glycerin case the swirling instability does not appear at all, remaining in a plane wave sloshing regime. This was further checked by extending that simulation up to 150 periods. It is worth remarking that, for all the swirling cases, the non-dimensional force F_x significantly increases in amplitude after the development of swirling instability.

The orbital evolution of the horizontal force components for the four fluids is reported in Fig. 5 as a function of time. Again for water, sunflower and castor oil the development of the swirling instability is evident. As for the water case, the high intensity of the free surface fragmentation, the frequent occurrence of roof impacts and several breaking events appear as a chaotic path of the orbit evolution in the quasi-periodic flow regime. Conversely, in the oil cases, the orbits are much smoother and strictly follow a periodic path. On the contrary,

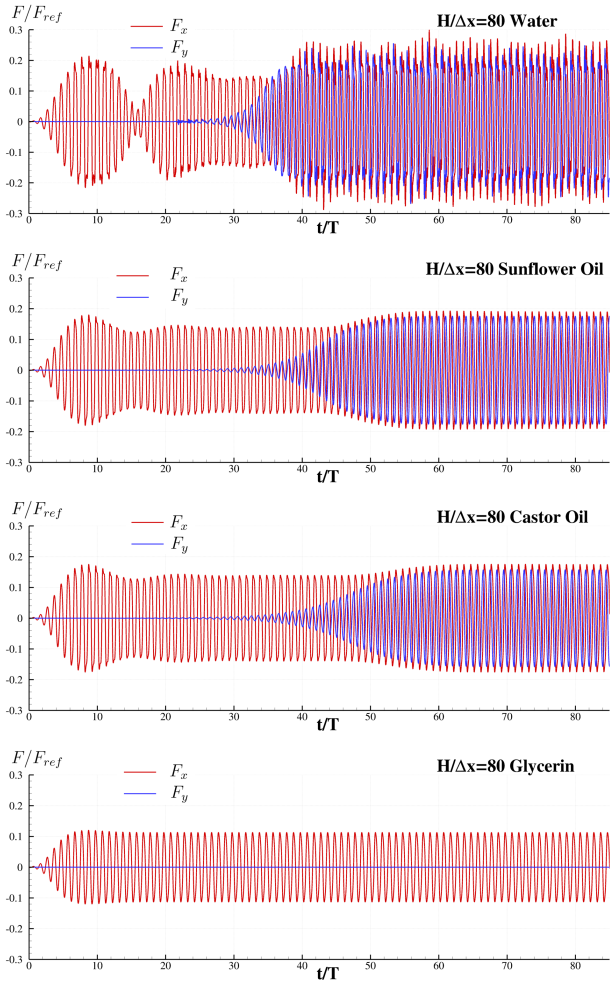

Fig. 4. Time history of horizontal force components, F_x and F_y, for the four different liquids. Force are made non-dimensional through the liquid weight $F_{ref} = m_l\, g$.

glycerin oscillates periodically only in the x direction during the entire simulation.

The time evolution of the forces in the quasi-periodic regime creates orbits that can be inscribed in a parallelogram. The height of this parallelogram provides an indication about the intensity of the instability. In addition, the distance between the initial orbitals (coloured in yellow and red in Fig. 5) is linked to the celerity with which the swirling instability takes place. A further comment can be made on the inclination of the parallelogram. The direction of the inclination gives information about the fluid rotation direction: water and castor oil cases feature a clockwise rotation whereas the sunflower oil anti-clockwise one.

D. Energy dissipation

In the present section the time evolution of the main energy components is discussed. As introduced in Sec. II-D the energy balance is given by three primary terms:

$$\mathcal{E}_M - \mathcal{W}_{NF} = \mathcal{E}_{diss}$$

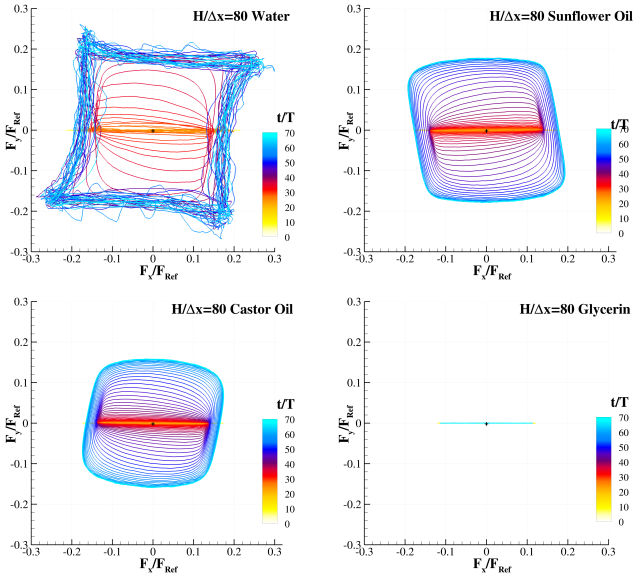

Fig. 5. Orbital evolution of the horizontal force components for the four liquids.

where $\mathcal{E}_M$ is the mechanical energy of the fluid in the Non-inertial frame of reference (Ni-FoR), $\mathcal{W}_{NF}$ is the work performed by the non-inertial forces and $\mathcal{E}_{diss}$ is the energy dissipated by the fluid.

Fig. 6 shows the time behaviour of the three energy components for the four liquids. As for the water test-case, a change of steepness of E_{diss} is well visible when entering in the regime III and IV discussed in Sec. III-B. Regime III is characterised by breaking waves and wall impact events which increase the dissipation rate. However, when the regime IV commences, corresponding to the establishment of the swirling motion, the dissipation rate reaches its maximum. The slope of $\mathcal{E}_{diss}$ remains almost constant in time being the flow in quasi-periodic regime. The double steepness behaviour of E_{diss} linked to the regime III and IV is evident also for the sunflower and castor oils.

A different behaviour characterises the glycerin test-case, for which E_{diss} exhibits a constant steepness just after a few oscillation periods. For this case the dissipation mechanism is mainly linked to the viscous forces in the boundary layer regions as the free-surface motion is smooth and periodic for the entire simulation. As underlined in [12], the dissipation linked to the Viscous Boundary Layer (VBL) and the violent free-surface motion are two completely different mechanisms: in the water test-case the former is negligible; conversely, in the glycerin test-case the dissipation is essentially driven by the VBL. For the sunflower and castor oils the two mechanisms are coupled in a complex and non-linear way.

Table II reports the dissipation rate $\mathcal{P}_{diss}$ in Watt for the four liquids and for three different spatial resolutions. The tendency is clear: the water test-case presents the higher $\mathcal{P}_{diss}$ for all the simulations. Clearly, the liquids characterised by lower viscosity feature the highest dissipation rate thanks to

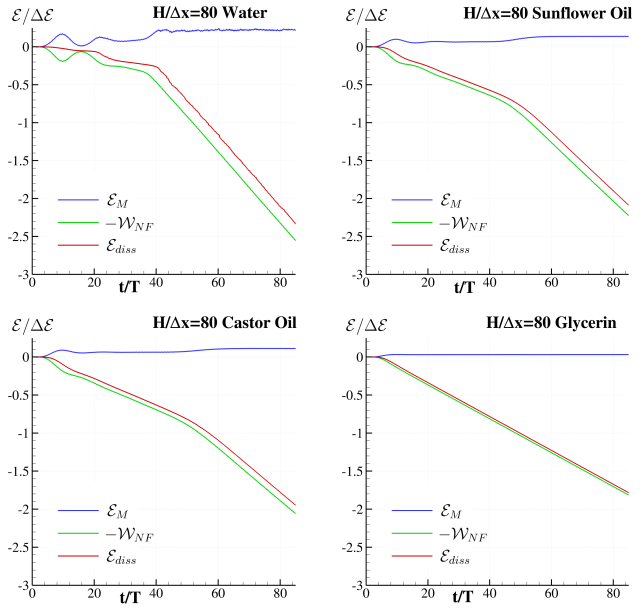

Fig. 6. Time evolution of the fluid mechanical energy $\mathcal{E}_M$ (evaluated in the Non-inertial frame of reference), the work $\mathcal{W}_{NF}$ performed by the non-inertial forces and the energy dissipated by the fluid $\mathcal{E}_{diss}$ for the four different test-cases.

$\mathcal{P}_{diss}$ (W)	Water	Sunflower Oil	Castor Oil	Glycerin
$N = 40$	7.98	5.61	5.45	4.87
$N = 60$	7.66	5.79	5.44	4.77
$N = 80$	7.62	5.88	5.44	4.76

TABLE II
RATE OF DISSIPATED ENERGY $\mathcal{P}_{diss}$ EXPRESSED IN WATT IN THE QUASI-PERIODIC REGIME FOR THE FOUR LIQUIDS AT DIFFERENT SPATIAL RESOLUTION $N = H/\Delta x$.

the large motion of the free-surface and the multiple impact events.

The dissipation rates of table II are also reported in Fig. 7 against their associated Reynolds numbers in logarithmic scale. Even if the considered Reynolds numbers are few, it is evident that the rate of dissipation increases with Re even if the dependency is rather complex. This is mainly linked to the combination of the two dissipation mechanisms: (i) the one related with the free-surface motion/fragmentation and (ii) the one linked to the VBL. This topic deserves further investigations with a more regular sampling of the considered Reynolds range and simulations with higher spatial resolutions for the largest Re numbers.

IV. Conclusions

Swirling waves instability is numerically investigated using an enhanced version of the Smoothed Particle Hydrodynamic (SPH) model called δ-LES-SPH model. The flow is studied inside a 3D square-base tank with filling ratio of 50.8% forced with a horizontal motion at a frequency equal to the resonant one. The focus is on how viscosity influences this instability, considering four different liquids: water, sunflower oil, castor oil and glycerine. The resulting Reynolds numbers span from

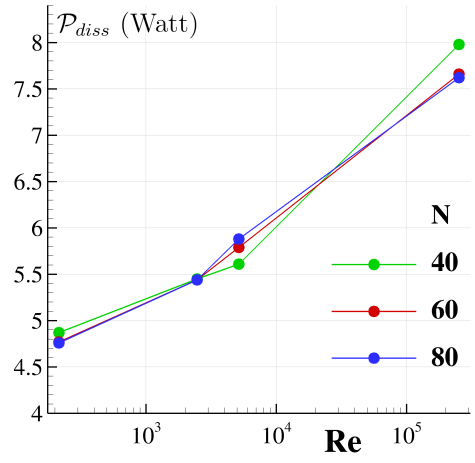

Fig. 7. Rate of dissipated energy $\mathcal{P}_{diss}$in the quasi-periodic regime for the four liquids at different spatial resolution $N = H/\Delta x$.

about 200 up to 250,000

Because of the highly non-linear behaviour of the sloshing phenomenon we showed that the swirling instability, when it is not inhibited by the viscosity, can be reached only after a long time transient stage. Thanks to the conservation properties of the SPH models, these simulations are obtained without accumulating significant errors on the main conservation quantities.

The results show that energy dissipation largely increases when the swirling instability takes place. The dissipation phenomenon is strictly linked to the free-surface fragmentation, occurring at higher Reynolds numbers. This is the case of water that exhibits a faster and more pronounced swirling instability and dissipates more energy during its rotating motion than the other three liquids characterised by higher viscosity. It is evident from the present work that the dependency of the dissipation rate on the fluid viscosity is complex across the considered range of Reynolds numbers. However, as only four test-cases were analysed, this topic deserves future investigations to describe more in details such a relation.

Acknowledgements

The work was supported by the “Siemens Digital Industries Software Chair” and simulation were performed by using HPC resources of the Centrale Nantes Supercomputing Centre on the cluster Liger.

The work was also partially supported by the SLOWD project which received funding from the European Union’s Horizon 2020 research and innovation programme under grant agreement No 815044, and partially supported by the Italian “Ministero dell’Ambiente e Sicurezza Energetica” under the Grant Agreement “RdS PTR 2022–2024 - Energia elettrica dal mare.

References

[1] M. Antuono, A. Colagrossi, and S. Marrone. Numerical diffusive terms in weakly-compressible SPH schemes. *Computer Physics Communications*, 183(12):2570–2580, 2012.

[2] M. Antuono, S. Marrone, A. Di Mascio, and A. Colagrossi. Smoothed Particle Hydrodynamics method from a large eddy simulation perspective. Generalization to a quasi-lagrangian model. *Physics of Fluids*, 33(1):015102, 2021.

[3] M Antuono, C Pilloton, A Colagrossi, and D Durante. Clone particles: A simplified technique to enforce solid boundary conditions in SPH. *Computer Methods in Applied Mechanics and Engineering*, 409:115973, 2023.

[4] M Antuono, PN Sun, S Marrone, and A Colagrossi. The δ-ALE-SPH model: An arbitrary lagrangian-eulerian framework for the δ-SPH model with particle shifting technique. *Computers & Fluids*, 216:104806, 2021.

[5] Matteo Antuono, S Marrone, A Colagrossi, and B Bouscasse. Energy balance in the δ-SPH scheme. *Computer Methods in Applied Mechanics and Engineering*, 289:209–226, 2015.

[6] Christophe Bailly and Geneviève Comte-Bellot. *The Dynamics of Isotropic Turbulence*, pages 179–210. Springer International Publishing, 2015.

[7] B. Bouscasse, A. Colagrossi, A. Souto-Iglesias, and J.L. Cercos-Pita. Mechanical energy dissipation induced by sloshing and wave breaking in a fully coupled angular motion system. I. theoretical formulation and numerical investigation. *Physics of Fluids*, 26(3):033103, 2014.

[8] J Calderon-Sanchez, J Martinez-Carrascal, LM González-Gutiérrez, and A Colagrossi. A global analysis of a coupled violent vertical sloshing problem using an sph methodology. *Engineering Applications of Computational Fluid Mechanics*, 15(1):865–888, 2021.

[9] Bang-Fuh Chen, Chih-Hua Wu, and Odd Magnus Faltinsen. The mechanism of switching direction of swirling sloshing waves. *Journal of Fluid Mechanics*, 954:A2, 2023.

[10] Andrea Colagrossi, Matteo Antuono, and David Le Touzé. Theoretical considerations on the free-surface role in the smoothed-particle-hydrodynamics model. *Physical Review E*, 79(5):056701, 2009.

[11] Andrea Colagrossi, Matteo Antuono, Antonio Souto-Iglesias, and David Le Touzé. Theoretical analysis and numerical verification of the consistency of viscous smoothed-particle-hydrodynamics formulations in simulating free-surface flows. *Physical Review E*, 84(2):026705, 2011.

[12] Andrea Colagrossi, Benjamin Bouscasse, and Salvatore Marrone. Energy-decomposition analysis for viscous free-surface flows. *Physical Review E*, 92(5):053003, 2015.

[13] Odd M Faltinsen, Oleksandr E Lagodzinskyi, and Alexander N Timokha. Resonant three-dimensional nonlinear sloshing in a square base basin. part 5. three-dimensional non-parametric tank forcing. *Journal of Fluid Mechanics*, 894:A10, 2020.

[14] Odd M Faltinsen, Olav F Rognebakke, and Alexander N Timokha. Resonant three-dimensional nonlinear sloshing in a square-base basin. *Journal of Fluid Mechanics*, 487:1–42, 2003.

[15] Odd Magnus Faltinsen and Alexander N Timokha. *Sloshing*, volume 577. Cambridge university press Cambridge, 2009.

[16] OM Faltinsen, OF Rognebakke, and AN Timokha. Classification of three-dimensional nonlinear sloshing in a square-base tank with finite depth. *Journal of Fluids and structures*, 20(1):81–103, 2005.

[17] Xin Jin, Jinbo Tang, Xiaochun Tang, Shuo Mi, Jiaxin Wu, Mingming Liu, and Zongliu Huang. Effect of viscosity on sloshing in a rectangular tank with intermediate liquid depth. *Experimental Thermal and Fluid Science*, 118:110148, 2020.

[18] S.J. Lind, R. Xu, P.K. Stansby, and B.D. Rogers. Incompressible smoothed particle hydrodynamics for free-surface flows: A generalised diffusion-based algorithm for stability and validations for impulsive flows and propagating waves. *Journal of Computational Physics*, 231(4):1499–1523, 2012.

[19] Edmond YM Lo and Songdong Shao. Simulation of near-shore solitary wave mechanics by an incompressible sph method. *Applied Ocean Research*, 24(5):275–286, 2002.

[20] Fabricio Macia, Matteo Antuono, Leo M González-Gutiérriez, and Andrea Colagrossi. Theoretical analysis of the no-slip boundary condition enforcement in sph methods. *Progress of theoretical physics*, 125(6):1091–1121, 2011.

[21] Leon Cillie Malan, Chiara Pilloton, Andrea Colagrossi, and Arnaud George Malan. Numerical calculation of slosh dissipation. *Applied Sciences*, 12(23):12390, 2022.

[22] S. Marrone, A. Colagrossi, J. Calderon-Sanchez, and J. Martinez-Carrascal. Numerical study on the dissipation mechanisms in sloshing flows induced by violent and high-frequency accelerations. II. comparison against experimental data. *Phys. Rev. Fluids*, 6:114802, Nov 2021.

[23] S. Marrone, A. Colagrossi, F. Gambioli, and L. González-Gutiérrez. Numerical study on the dissipation mechanisms in sloshing flows induced by violent and high-frequency accelerations. I. theoretical formulation and numerical investigation. *Phys. Rev. Fluids*, 6:114801, Nov 2021.

[24] S Marrone, F Saltari, J Michel, and F Mastroddi. Sph modelling of dissipative sloshing flows under violent vertical harmonic excitation. *Journal of Fluids and Structures*, 119:103877, 2023.

[25] D.D. Meringolo, S. Marrone, A. Colagrossi, and Y. Liu. A dynamic δ-SPH model: How to get rid of diffusive parameter tuning. *Computers & Fluids*, 179:334–355, 2019.

[26] J Michel, M Antuono, G Oger, and S Marrone. Energy balance in quasi-lagrangian riemann-based sph schemes. *Computer Methods in Applied Mechanics and Engineering*, 410:116015, 2023.

[27] J Michel, D Durante, A Colagrossi, and S Marrone. Energy dissipation in violent three-dimensional sloshing flows induced by high-frequency vertical accelerations. *Physics of Fluids*, 34(10):102114, 2022.

[28] Joe J Monaghan. Smoothed particle hydrodynamics. *Reports on progress in physics*, 68(8):1703, 2005.

[29] Ruairi M Nestor, Mihai Basa, Martin Lastiwka, and Nathan J Quinlan. Extension of the finite volume particle method to viscous flow. *Journal of Computational Physics*, 228(5):1733–1749, 2009.

[30] G. Oger, S. Marrone, D. Le Touzé, and M. De Leffe. SPH accuracy improvement through the combination of a quasi-Lagrangian shifting transport velocity and consistent ALE formalisms. *Journal of Computational Physics*, 313:76–98, 2016.

[31] C Pilloton, A Bardazzi, A Colagrossi, and S Marrone. SPH method for long-time simulations of sloshing flows in lng tanks. *European Journal of Mechanics-B/Fluids*, 93:65–92, 2022.

[32] N.J. Quinlan, M. Lastiwka, and M. Basa. Truncation error in mesh-free particle methods. *International Journal for Numerical Methods in Engineering*, 66(13):2064–2085, 2006.

[33] Benedict D Rogers and Robert A Dalrymple. SPH modeling of breaking waves. In *Coastal Engineering 2004: (In 4 Volumes)*, pages 415–427. World Scientific, 2005.

[34] J. Smagorinsky. General circulation experiments with the primitive equations: I. the basic experiment. *Monthly weather review*, 91(3):99–164, 1963.

[35] Andrei Tsarau, Claudio Lugni, Alessia Lucarelli, David Kristiansen, and Pål Lader. Sloshing in a rotating liquid inside a closed sea cage for fish farming. *Physics of Fluids*, 33(3):037114, 2021.

[36] H. Wendland. Piecewise polynomial, positive definite and compactly supported radial functions of minimal degree. *Adv. Comput. Math.*, 4(4):389–396, 1995.

[37] Chih-Hua Wu, Tin-Kan Hung, and Bang-Fuh Chen. Kinematic, dynamic and energy characteristics of swirling sloshing waves. *Ocean Engineering*, 272:113875, 2023.